Cell Reports
Article

Cell PRESS
Open ACCESS

SIRT1 Suppresses the Epithelial-to-Mesenchymal Transition in Cancer Metastasis and Organ Fibrosis

Petra Simic,[1] Eric O. Williams,[1] Eric L. Bell,[1] Jing Jing Gong,[1] Michael Bonkowski,[1] and Leonard Guarente[1,*]
[1]Glenn Laboratory for the Science of Aging and Department of Biology, Massachusetts Institute of Technology, Cambridge, MA 02139, USA
*Correspondence: leng@mit.edu
http://dx.doi.org/10.1016/j.celrep.2013.03.019

SUMMARY

The epithelial-to-mesenchymal transition (EMT) is important for the development of cancer metastases and organ fibrosis, conditions prevalent in aging. Because sirtuins affect the pathology of aging, we tested the effect of *SirT1* on EMT. Reduced SIRT1 levels in HMLER breast cancer cells led to increased metastases in nude mice, and the loss of SIRT1 in kidney tubular epithelial cells exacerbated injury-induced kidney fibrosis. SIRT1 reduces EMT in cancer and fibrosis by deacetylating Smad4 and repressing the effect of TGF-β signaling on MMP7, a Smad4 target gene. Consequently, less E-cadherin is cleaved from the cell surface and β-catenin remains bound to E-cadherin at the cell-cell junctions. Our findings suggest that the SIRT1/Smad4/β-catenin axis may be a target for diseases driven by EMT.

INTRODUCTION

The epithelial-to-mesenchymal transition (EMT) is a process in which epithelial cells lose cell-adhesive properties, repress E-cadherin expression, and increase mesenchymal gene expression and cell mobility. It is essential for three distinct biological processes: embryogenesis, organ fibrosis, and cancer metastases (Kalluri and Weinberg, 2009).

In cancer, EMT enables carcinoma cells to acquire cellular traits associated with high-grade malignancy and metastasis (Brabletz et al., 2005; Singh and Settleman, 2010). Some of the epithelial cells that enter EMT acquire the properties of stem cells (Mani et al., 2008; Morel et al., 2008). Importantly, this includes the potential for self-renewal, which may facilitate the formation of secondary tumors by disseminating cancer cells. EMT-derived migratory cancer cells establish secondary colonies at distant sites that resemble, at the histopathological level, the primary tumor from which they arose, suggesting that metastasizing cancer cells shed their mesenchymal phenotype via a mesenchymal to epithelial transition (MET) during the colonization process (Kalluri and Weinberg, 2009; Yao et al., 2011).

EMT was also proposed to occur in fibrosis of kidney, liver, heart, lung, and intestine (Potenta et al., 2008; Zeisberg et al., 2007; Kim et al., 2006). However, recent studies raised serious doubts about the existence of EMT in kidney fibrosis (Humphreys et al., 2010; Li et al., 2010b).

EMT in cancer progression and organ fibrosis is associated with aging (Mani et al., 2008; Chaturvedi and Hass, 2011; Pannarale et al., 2010). Indeed, aging is one of the single most important risk factors associated with cancer with nearly 65% of cancers occurring in patients ≥65 years old (Ertel et al., 2012). Similarly, fibrosis is a hallmark of pathogenesis associated with aging in many organs (Abrass et al., 1995).

Sirtuins are highly conserved nicotinamide-adenine-dinucleotide -dependent deacetylases that were shown to regulate lifespan in lower organisms (Tissenbaum and Guarente, 2001; Viswanathan and Guarente, 2011) and affect diseases of aging in mammals, such as diabetes, inflammation, and neurodegenerative diseases (Donmez and Guarente, 2010). The Sir2 ortholog SIRT1 is known to deacetylate transcription factors that govern pathways important for aging and diseases (Imai et al., 2000; Guarente, 2011).

Furthermore, calorie restriction protects against breast cancer (Nogueira et al., 2012), as well as against fibrotic kidney failure (Tapp et al., 1989) via SIRT1 (Kume et al., 2010). Indeed, there is a strong link between sirtuins and many of the effects of calorie restriction (Lin et al., 2000; Guarente and Picard, 2005), hinting at a possible relationship between mammalian SIRT1 and EMT. The role of SIRT1 in cancer has been shown in several studies to be cell type dependent and complex (see Discussion). Here, we investigated the role of SIRT1 in EMT in cancer metastasis and fibrosis. For this purpose, we analyzed the metastatic potential of breast cancer cells with or without SIRT1 after implantation into nude mice. We also probed the role of SIRT1 in long-term effects of ischemia reperfusion on kidney fibrosis in mice with varying levels of SIRT1 expression in tubular epithelial cells. After observing significant effects in these systems, we demonstrated that SIRT1 restrains the transforming-growth-factor (TGF)-β-signaling pathway, which is known to drive EMT. Our findings cast light on links between sirtuins and disease states abetted by the EMT.

RESULTS

Decrease in SIRT1 Level Promotes Breast Cancer Metastases via EMT

We initially tested the effect of SIRT1 on EMT in breast cancer cells. HMLER cells are primary human mammary epithelial cells (HMECs), which express the telomerase catalytic subunit, SV40

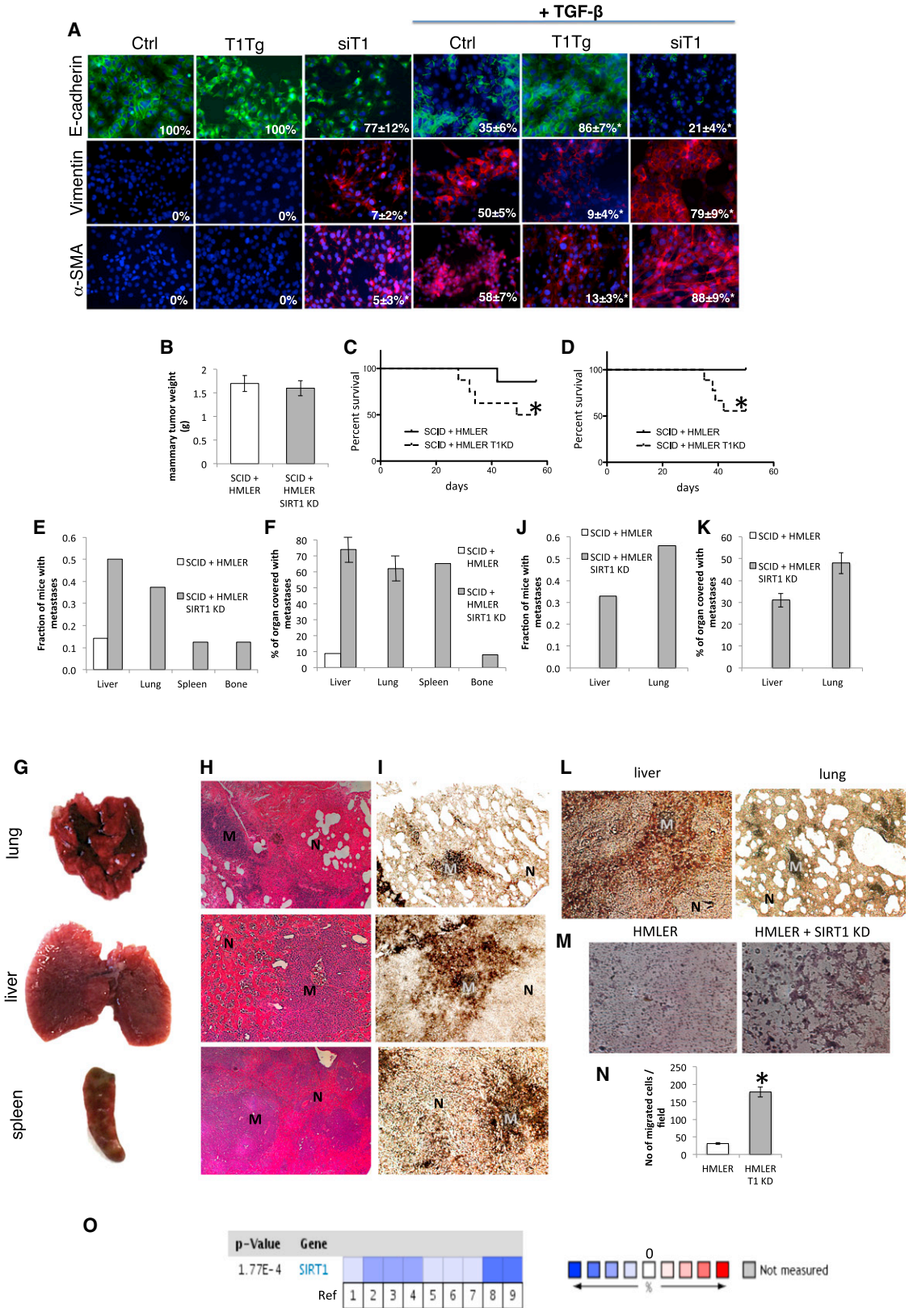

(legend on next page)

large T and small t antigens (HMLE cells), and an oncogenic allele of H-Ras, H-Ras^{V12} (Elenbaas et al., 2001). These cells are tumorigenic when injected subcutaneously or into the mammary glands of immunocompromised mice but have very low metastatic potential (Elenbaas et al., 2001, Ince et al., 2007). Treatment of HMLER cells with TGF-β led to transition of epithelial to mesenchymal cells as shown by a reduction of E-cadherin (epithelial marker) and an increase in vimentin (mesenchymal marker, Figure 1A). Overexpression of *SIRT1* reduced EMT, while repression of *SIRT1* by small interfering RNA (siRNA) increased EMT of HMLER cells in these assays (Figures 1A and S1A). Similar albeit less dramatic results were repeated in another breast cancer line MDA-MB231 (Figure S1B).

HMLER cells were stably transfected with the control vector or knockdown construct for *SIRT1* (*SIRT1* KD) (Figure S1C). A group of 15 mice were implanted with HMLER cells in the mammary fat pad of nude mice (seven with control and eight with HMLER SIRT1 KD cells), where they both grew mammary tumors similar in size (Figure 1B). However, nude mice with SIRT1 KD tumors had significantly reduced survival, with only 50% of mice surviving until 8 weeks following the implantation of tumor cells as compared to 86% survival in mice with wild-type tumors (Figure 1C). In a second trial, 17 mice (eight control and nine HMLER *SIRT1* KD implanted cells) showed a similar pattern, 56% survival in mice with *SIRT1* KD tumors and 100% survival in mice with wild-type tumors 7.5 weeks following tumor implantation (Figure 1D). Upon dissection, it was revealed in the first trial that seven out of eight mice with *SIRT1* KD tumors had multiple metastases, in liver (50% of mice), lung (38% of mice), spleen (13% of mice), and bone (13% of mice), while only one mouse out of seven had a single liver metastasis after implantation of wild-type tumor cells (Figure 1E). Metastasis burden analysis showed a substantial portion of liver, lung, and spleen surface covered with metastases in mice bearing *SIRT1* KD tumors (Figures 1F and 1G). Histology of these organs showed the purely differentiated phenotype characteristic of HMLER cells (Figure 1H). The origin of metastasis was additionally confirmed to be HMLER cells with immunohistochemical staining of large T antigen, used for transformation of HMEC to HMLER cells (Figure 1I). In the second experiment, seven out of nine mice with *SIRT1* KD tumors had metastases, 56% in lung and 33% in liver (Figure 1J), with 31%–48% of organs covered with metastases (Figure 1K). The HMLER origin of metastases was confirmed by immunohistochemical staining of large T antigen (Figure 1L) and scoring the GFP marker present in these cells (Figure S1D). None of the mice with HMLER wild-type tumors developed metastases in this experiment (Figures 1J and 1K). SIRT1 levels in the knockdown remained low in metastases as well as in primary tumors (Figure S1E). To determine migratory and invasive abilities of cells more directly, we used Boyden chamber assays. Whereas control cells were minimally motile and invasive, *SIRT1* KD cells showed a significant increase in both motility and invasiveness through Matrigel-coated membranes (Figures 1M and 1N). Taken together, these results indicate that knocking down *SIRT1* in breast cancer cells promotes EMT, cancer cell invasiveness, metastases, and increased mortality of nude mice.

To further confirm the effect of *SIRT1* on breast cancer metastases, we performed meta-analysis of SIRT1 expression in all breast cancer clinical studies in the Oncomine human cancer gene expression database, which includes 12 trials with 143 control and 1,181 breast cancer tissues (http://www.oncomine.com). We used the cutoff value of $p = 0.01$ for significance of any change in SIRT1 expression in any direction. Six out of 12 studies (nine out of 35 total comparisons) showed a significant change in *SIRT1* expression, and strikingly *SIRT1* was downregulated in all nine comparisons (fold change −1.216 to −4.822; Figure 1O; Table S1).

Loss of SIRT1 Leads to Kidney Fibrosis via EMT

We next wished to test a possible role of SIRT1 in EMT in a completely different context from tumor metastasis by using

Figure 1. The Role of SIRT1 in EMT of Breast Cancer Metastases

(A) Immunofluorescence staining of HMLER cells with E-cadherin, vimentin, and α-SMA 8 days following the treatment with TGF-β 5 ng/ml (63× magnification, DAPI staining of nuclei). Numbers in the bottom-right corners of images represent percentage of E-cadherin, vimentin, and α-SMA-positive cells over total number of cells per slide (n = 3 slides per group), shown as average ± SD, *$p < 0.05$, ANOVA Dunnett test, versus Ctrl treated with TGF-β; T1Tg, HMLER cells overexpressing *SIRT1*; siT1, HMLER cells with knockdown for *SIRT1*; Ctrl, control HMLER cells.

(B) Orthotopic mammary tumor weight following the termination of experiment.

(C and D) Survival of SCID mice up to 8 weeks (trial 1, left) and 7.5 weeks (trial 2, right) following the implantation of HMLER control and HMLER *SIRT1* KD cells. *$p \leq 0.05$ log-rank test versus HMLER control cells.

(E) Fraction of mice with metastases in different organs 8 weeks following the implantation of HMLER control cells and HMLER *SIRT1* KD cells (trial 1).

(F) Quantification of total organ metastasis burden (trial 1). Bars represent SD.

(G) Representative macroscopic images of mouse lung, liver, and spleen with visible metastatic nodules after implantation of HMLER *SIRT1* KD cells in SCID mice.

(H) Hemalaun-eosin staining of mouse lung, liver, and spleen sections. M, metastatic nodule; N, normal tissue.

(I) Representative immunohistochemical staining of sections with anti-large T antibody from the same set of organs. M, metastatic nodule; N, normal tissue.

(J) Fraction of mice with metastases in different organs 7.5 weeks following the implantation of HMLER control cells and HMLER *SIRT1* KD cells (trial 2).

(K) Quantification of total organ metastasis burden (trial 2). Bars represent SD.

(L) Representative immunohistochemical staining of sections with anti-large T antibody from the liver and lung (trial 2). M, metastatic nodule; N, normal tissue.

(M and N) HMLER and HMLER *SIRT1* KD cells were induced to move and invade through Matrigel-coated transwell membranes. After 16 hr, the migrated cells were fixed, stained, and photographed. Representative photographs of transwell membranes showing stained migrated cells. (M) Quantification of (N) done by counting the number of migrated cells. Columns, mean of triplicate assays; bars, SD; *$p < 0.05$, t test.

(O) Meta-analysis of *SIRT1* expression of 12 breast cancer clinical trials using Oncomine database (cutoff for significant SIRT1 change was $p = 0.01$). Blue quadrants represent downregulation of *SIRT1* and red upregulation. References are in Table S1.

See also Figure S1.

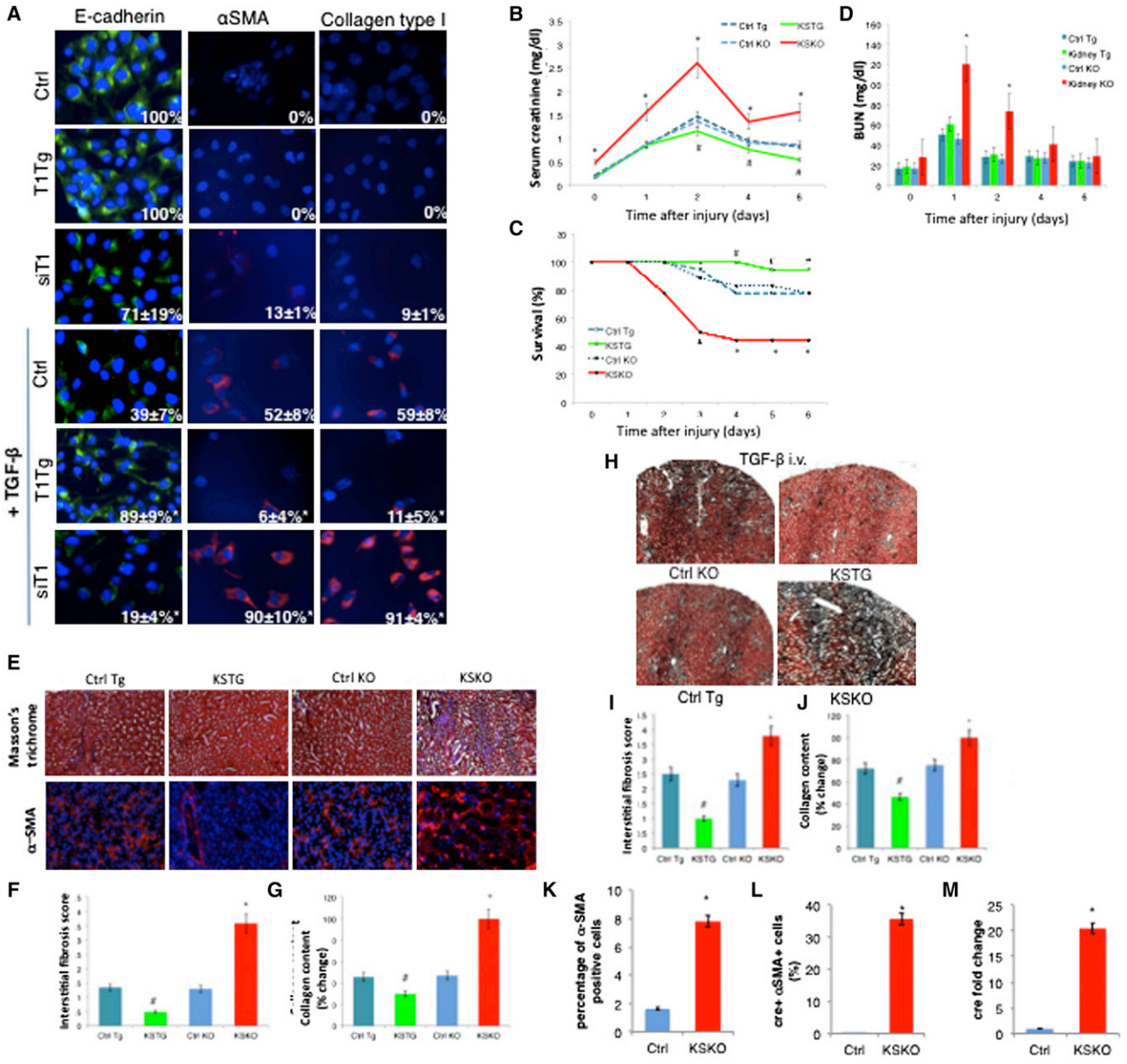

Figure 2. The Role of SIRT1 in EMT of Kidney Epithelial Cells and Kidney Fibrosis In Vivo

(A) Immunofluorescent staining of HK-2 cells with E-cadherin, α-smooth muscle actin (α-SMA), and collagen type I 48 hr following the treatment with TGF-β 5 ng/ml (63× magnification, DAPI staining of nuclei). Numbers in the right bottom corners of images represent percentage of E-cadherin, α-SMA, or collagen-type-I-positive cells over total number of cells per slide (n = 3 slides per group), shown as average ± SD, *p < 0.05, ANOVA Dunnett test versus Ctrl treated with TGF-β; T1Tg, HK-2 cells overexpressing SIRT1; siT1, HK-2 cells with knockdown for *SIRT1*; Ctrl, control HK-2 cells.

(B) Changes of serum creatinine over time following AKI (n = 12 for each time point).

(C) Survival following the AKI. *p ≤ 0.05 versus Ctrl KO, #p ≤ 0.05 versus Ctrl Tg, log-rank test.

(D) Blood urea nitrogen (BUN) values over time (n = 12 for each time point).

(E) Masson's trichrome staining showing mesenchymal tissue in blue and α-SMA immunofluorescent staining for myofibroblasts in red (magnification 20×, n = 6 per group).

(F) Interstitial fibrosis score of Masson's trichrome-stained kidney sections at 6 weeks following the AKI (n = 6 per group).

(G) Collagen content in kidneys 6 weeks following the AKI measured by Sircol assay (n = 6 per group).

(H) Masson's trichrome staining of kidneys after 4 days of treatment with TGF-β 100 μg/kg/day intravenously (magnification 5×).

(I) Interstitial fibrosis score of Masson's trichrome-stained kidney slides from (H).

(J) Collagen content in kidneys after 4 days of treatment with TGF-β 100 μg/kg/day intravenously, as determined by Sircol collagen assay. *Significantly different from Ctrl KO, #significantly different from Ctrl Tg, ANOVA Dunnett test, p ≤ 0.05. Error bars represent SD. KSTG, kidney-specific transgenic mice; Ctrl Tg, control for KSTG; KSKO, kidney-specific knockout mice; Ctrl KO, control for KSKO mice.

(legend continued on next page)

kidney epithelial cells and a kidney injury model in mice expressing reduced or elevated levels of SIRT1 (Figure S2A).

Treatment of kidney epithelial HK-2 cells with TGF-β or aristocholic acid, to mimic kidney injury, gave rise to cells with mesenchymal phenotypes, as shown by an increase in cells positive for α-smooth muscle actin (α-SMA) and collagen type I (markers for mesenchymal cells) and a decrease in cells positive for E-cadherin, an epithelial marker (Figures 2A and S2B). Overexpression of *SIRT1* in epithelial HK-2 cells led to a repression of EMT, as seen by a reduction in α-SMA and collagen-positive cells. Moreover, preservation of the epithelial phenotype was confirmed by the continued expression of E-cadherin after the treatments with TGF-β or aristocholic acid (Figures 2A and S2B). Conversely, loss of *SIRT1* by siRNA in HK-2 kidney epithelial cells increased the EMT, as assessed by an increase in α-SMA and collagen-positive cells and a decrease in E-cadherin-positive cells (Figures 2A and S2B).

To test the effect of SIRT1 on kidney function in vivo, we studied the acute kidney injury (AKI) model of ischemia reperfusion in kidney-specific knockout mice (KSKO) and kidney-specific transgenic mice (KSTG) mice. KSKO mice eliminate *SIRT1* from kidney collective tubular epithelial cells, while KSTG increase *SIRT1* expression in these same cells (Figures S2C–S2E). At the baseline, KSTG and KSKO had comparable body weight and levels of serum electrolytes (Figures S2F and S2G). Serum creatinine values, representing kidney function, were increased in KSKO mice before the AKI (Figure 2B), suggesting the requirement of SIRT1 for maintenance of tubular epithelial function even in the absence of injury. After clamping the renal arteries to induce injury, the increase of the serum creatinine was much more pronounced in the absence of SIRT1 from kidney tubules (Figure 2B). There was an improvement in creatinine values in KSKO mice on day 4 following the AKI, since the mice with the worst glomerular function had died by that time (Figure 2C). KSTG showed better kidney function parameters with significantly lower creatinine values as compared to the control animals. Blood urea nitrogen (BUN) paralleled serum creatinine measurements (Figure 2D). Most importantly, overexpression of *SIRT1* in kidney tubules protected animals from dying after AKI, while deletion exacerbated mortality (Figure 2C). Histological examination of the injured kidneys demonstrated destruction of the tubular basement membrane and disorientation of epithelial tubular cells following the AKI. These phenotypes were significantly more pronounced in KSKO and reduced in KSTG mice (Figures S2H and S2I).

Since aging impedes the recovery from AKI and predisposes to irreversible damage of kidneys (Abrass et al., 1995), we investigated the effect of SIRT1 on fibrosis in kidneys without the injury and on progression of AKI to tubulointerstitial fibrosis and development of chronic kidney damage (CKD) by following the KSKO and KSTG mice for 6 weeks after the AKI. At baseline, KSKO mice had a minimal increase in kidney fibrosis (Figure S2J). After the AKI, KSKO mice had significantly worse kidney function as detected by the increased serum creatinine (Figure S2K) and BUN (Figure S2L), more kidney fibrosis (Figure 2F) as confirmed by Masson's trichrome staining for connective tissue and α-SMA staining for myofibroblasts (Figure 2E) and increased kidney collagen content (Figure 2G). In contrast, KSTG showed improvement compared to the control mice subjected to kidney injury. In summary, the elimination of *SIRT1* predisposes kidneys to fibrosis and progression from AKI to CKD, while overexpression of SIRT1 in kidney tubules improves the recovery after the AKI and slows the progression toward CKD.

Our findings above suggest that SIRT1 represses kidney fibrosis. Since it is known that the TGF-β pathway induces fibrosis (Ledbetter et al., 2000), we tested whether SIRT1 repression of TGF-β was sufficient to explain the observed repression in fibrosis. We treated wild-type, KSKO, and KSTG mice with 100 μg/kg of TGF-β intravenously for 4 days. In mice treated with TGF-β, we recapitulated the effects of SIRT1 seen after AKI. Namely, KSTG mice showed less fibrosis on histology (Figures 2H and 2I) and less collagen (Figure 2J) in kidney tissues, and KSKO mice showed more fibrosis and collagen after the treatment with TGF-β. These results suggest that SIRT1 represses kidney fibrosis by repressing the TGF-β pathway.

To address whether EMT was likely to be involved in fibrosis in wild-type or KSKO kidneys, we FACS sorted α-SMA-positive cells after treatment with TGF-β to cause fibrosis, and found, as expected, 4.8-fold more positive (fibrotic) cells in kidneys of KSKO mice (Figure 2K). Since cre-recombinase expression in KSKO mice is driven by the kidney epithelial collecting tubule-specific *Hoxb7cre* promoter (Yu et al., 2002), we tested for EMT by FACS sorting the α-SMA-positive cells and testing for cre expression. Consistent with recent reports (Humphreys et al., 2010), almost none of sorted α-SMA-positive cells had cre recombinase (0.02%) in *SIRT1*$^{+/+}$ mice expressing cre, after the TGF-β treatment. In striking contrast, 35.7% of α-SMA-positive cells in KSKO treated with TGF-β expressed cre recombinase (Figure 2L). Quantitative RT-PCR also demonstrated vastly higher cre expression in α-SMA-positive cells of KSKO compared to wild-type (Figure 2M). These findings suggest that EMT is not the mechanism of kidney fibrosis in control animals as recently reported (Humphreys et al., 2010). However, EMT is induced at a very high frequency in fibrotic kidney tissue in the absence of SIRT1.

SIRT1 Deacetylates Smad4 and Represses the Activity of TGF-β Pathway on MMP7

Since MMP7 has been associated with aging and fibrosis in kidneys (Chen et al., 2007), we determined the levels of this protein in the various mice after AKI. In KSTG mice, there was significantly less expression of *MMP7* after AKI, while the expression

(K) Percentage of α-SMA-positive cells in kidneys of *SIRT1*$^{+/+}$ mice expressing the cre-recombinase (Ctrl) and KSKO mice detected by flow cytometry.
(L) Percentage of cre-recombinase-positive cells out of α-SMA-positive cells in kidneys of *SIRT1*$^{+/+}$ mice expressing cre-recombinase (Ctrl) and KSKO mice as detected by flow cytometry.
(M) Quantitative RT-PCR analysis of cre-recombinase expression in sorted α-SMA-positive cells from kidneys of *SIRT1*$^{+/+}$ mice expressing cre-recombinase (Ctrl) and KSKO mice.
Bars, SD, *$p < 0.05$ versus Ctrl, t test. See also Figure S2.

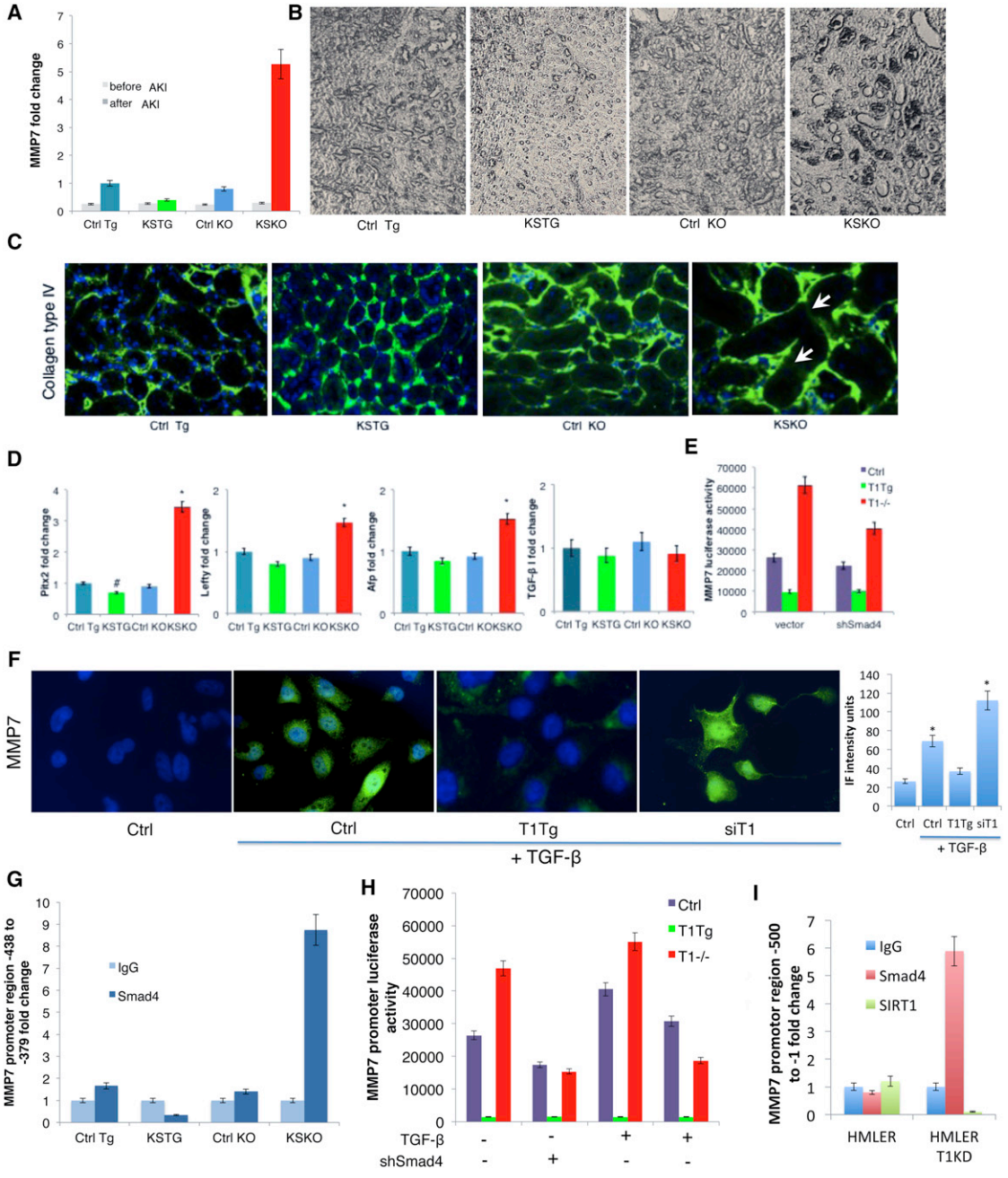

Figure 3. SIRT1 Represses the Activity of TGF-β Pathway on MMP7

(A) *MMP7* fold change detected by quantitative RT-PCR in kidneys 6 days following the AKI (n = 6 per group).

(B) Immunohistochemistry showing localization of MMP7 around tubules in kidneys 6 days following AKI (Vecta-stain, 5× magnification).

(C) Immunofluorescent staining for collagen type IV for tubular basement membrane and DAPI for nuclei in kidney sections 6 days following AKI (20× magnification). Numbers in the bottom-right corners of images represent percentage of collagen-IV-positive green area over total area (n = 3 slides per group), shown as average ± SD. Arrows depict destruction of collagen IV in the basement membrane.

(D) Quantitative RT-PCR expression of TGF-β I and some of TGF-β target genes—*Pitx2*. *Lefty* and *Afp*—in kidneys 6 days following AKI.

(E) Luciferase activity of *MMP7* promoter (−660 to −280) in wild-type, *SIRT1*$^{-/-}$ and *SIRT1*-overexpressing MEFs treated with TGF-β (2 ng/ml for 48 hr). Left, vector control; right, shRNA Smad4.

(F) MMP7 immunofluorescent staining of kidney epithelial tubular HK-2 cells treated with TGF-β 5 ng/ml for 48 hr (63× magnification, DAPI staining of nuclei). Bar graph is quantification of MMP7 immunofluorescence intensity by ImageJ. In each of the four groups, three to four different fields were analyzed. *Significantly different from Ctrl, ANOVA Dunnett test, $p \leq 0.05$. Error bars represent SD.

(G) Chromatin-immunoprecipitation on kidneys 6 days following the AKI with anti-Smad4 antibody or IgG. Different activity regions of the *MMP7* promoter are tested by quantitative RT-PCR using the appropriate primers (Table S2).

(legend continued on next page)

of *MMP7* was increased 5.7-fold in KSKO kidney (Figure 3A). Immunohistochemistry revealed increased levels of MMP7 protein at the basement membrane of collecting tubules in KSKO mice (Figure 3B). The increment of MMP7 in KSKO kidneys correlated with increased destruction of collagen IV, a basement membrane-specific target of MMP7, as shown by immunofluorescent staining (Figure 3C). Conversely, there was less MMP7 protein and less basal membrane destruction in kidneys from KSTG mice (Figures 3B and 3C). There were no significant changes in the expression of *MMP2* or *MMP9* (Figure S3A).

Since TGF-β signaling is the most significant pathway leading to EMT, cancer metastases, and fibrosis, we also analyzed the effect of SIRT1 levels on the TGF-β pathway. The expression of downstream genes involved in the TGF-β pathway was significantly increased in the absence of SIRT1 from kidney tubules after injury, as confirmed by quantitative RT-PCR expression of TGF-β pathway downstream targets *Pitx2*, *Lefty*, and *Afp* (Figure 3D). However, there was no significant change in TGF-β expression itself among all groups subjected to kidney injury (Figure 3D).

To address whether the SIRT1 regulation of MMP7 expression was via the TGF-β pathway, we first monitored MMP7 expression in HK-2 kidney epithelial cells that either overexpressed or had knocked down levels of SIRT1 (Figure S2A). Overexpression of SIRT1 reduced the levels of TGF-β-induced MMP7, while knockdown of SIRT1 increased levels (Figure 3F). To confirm that SIRT1 regulated MMP7 via TGF-β signaling, we next constructed a luciferase reporter driven by a large fragment of *MMP7* upstream DNA (−660 to −216) and tested it in wild-type, *SIRT1*$^{-/-}$, and *SIRT1*-overexpressing mouse embryonic fibroblasts (MEFs). This reporter showed a strong regulation by SIRT1, which was partially normalized by small hairpin RNA (shRNA) to *Smad4*, the transcription factor that responds to TGF-β signaling (Figures 3E and S3B).

The SIRT1 effects on TGF-β and MMP7 might occur via an interaction between the TGF-β-activated transcription factor Smad4 and a site in the *MMP7* promoter. To test this idea, we performed chromatin immunoprecipitation assay, which revealed a direct interaction of Smad4, with a specific region of *MMP7* promoter −438 to −379, but not with other promoter regions (Figures 3G and S3C). Critically, this interaction is greatly enhanced in the *SIRT1*$^{-/-}$ kidneys and reduced in kidneys overexpressing *SIRT1*. To further validate the relevance of this *MMP7* promoter site, we constructed a luciferase reporter with only the −438 to −379 region and tested it in MEFs. Luciferase levels were activated by TGF-β, and activation was higher in *SIRT1*$^{-/-}$ MEFs and blunted in *SIRT1*-overexpressing MEFs (Figure 3H). The increase in activity of this promoter in *SIRT1*$^{-/-}$ MEFs was eliminated by treating cells with shRNA for *Smad4*. We confirmed the interaction between Smad4 and the *MMP7* promoter by chromatin immunoprecipitation in HMLER T1KD cells (Figure 3I). There was no direct interaction of SIRT1 and the MMP7 promoter in HMLER cells (Figure 3I), suggesting SIRT1 may function by deacetylating Smad4. We also used a different assay for Smad4 activity—a Gal4 fusion to a Smad2/4 interacting motif from Fox H1 to recruit phosphorylated Smad2-Smad4 complexes to a Gal4 binding site that drives luciferase (Ross et al., 2006). Using this assay in the MEFs, there was again more activation of Smad2-Smad4 complex in the absence of SIRT1 and less activation in cells overexpressing SIRT1 (Figures S3D and S3E).

To test whether SIRT1 deacetylates Smad4, we immunoprecipitated Smad4 and also Smad2 from mouse kidneys and probed western blots with antibodies to the Smad proteins or acetyl lysine (Figure 4A). This experiment showed a clear increase in acetylation of Smad4 but not Smad2 in the KSKO kidneys. To investigate the effect of aging on the Smad4 pathway in wild-type kidneys, we tested the levels of SIRT1 protein and Smad4 acetylation in kidneys at different ages. Interestingly, there was a decrease in SIRT1 levels in kidneys from 2-year-old mice as compared to young mice at 3 months of age (Figure 4B). Moreover, there was a corresponding increase in Smad4 acetylation in aged kidneys (Figure 4B). We also observed an increase in acetylation of Smad4 in *SIRT1* KD HMLER cells (Figure 4C). Finally, SIRT1 and Smad4 were shown to interact at endogenous level in HMLER cells by coimmunoprecipitation (Figure S3F).

Furthermore, MMP7 protein levels were elevated in *SIRT1* KD HMLER cells (Figure 4D). Since MMP7 cleaves E-cadherin from the cell surface (Noë et al., 2001; Zheng et al., 2009), we tested the effect of SIRT1 on E-cadherin in HMLER cells. *SIRT1* KD HMLER cells showed modestly less E-cadherin on western blot analysis. This effect was blunted by the reduction of MMP7 levels, suggesting that *SIRT1* KD exerts its effect on E-cadherin via MMP7 (Figure 4D). Notably, TGF-β reduced E-cadherin in both, wild-type and *SIRT1* KD HMLER cells, but to a much greater extent in *SIRT1* KD cells, and this too was blunted by shRNA for *MMP7* (Figure 4D).

β-catenin is associated with the E-cadherin cytoplasmic tail, and loss of E-cadherin leads to translocation of β-catenin from adheren junctions to the nucleus (Onder et al., 2008). As *SIRT1* KD reduces E-cadherin levels in HMLER cells, we investigated whether this induced a change in the cellular localization of β-catenin upon TGF-β addition. Indeed, *SIRT1* KD led to translocation of β-catenin from the cell junctions (characteristic of epithelial cells) to nuclei (characteristic of mesenchymal cells, Kalluri and Weinberg, 2009) upon addition of TGF-β (Figures 4E and S4).

(H) Luciferase reporter assays of MEFs overexpressing *SIRT1* (T1TG), lacking *SIRT1* (T1−/−), or controls (Ctrl). Cells were transfected with luciferase reporter driven by the *MMP7* promoter region responsive to Smad4 (−438 to −379) and/or Smad4 shRNA, and were incubated with TGF-β 2 ng/ml for 48 hr and assayed as described in Experimental Procedures.

(I) Chromatin-immunoprecipitation on HMLER and HMLER T1KD cells with anti-Smad4, anti-SIRT1 antibody, or IgG. Different activity regions of the MMP7 promoter are tested by quantitative RT-PCR using the appropriate primers (Table S2).

Ctrl Tg, control for *SIRT1* kidney-specific transgenic mice; KSTG, kidney-specific transgenic mice; Ctrl KO, control for *SIRT1* kidney-specific knockout mice; KSKO, kidney-specific knockout mice. *Significantly different from Ctrl KO; #significantly different from Ctrl Tg, ANOVA Dunnett test, $p \leq 0.05$. Error bars represent SD. See also Figure S3.

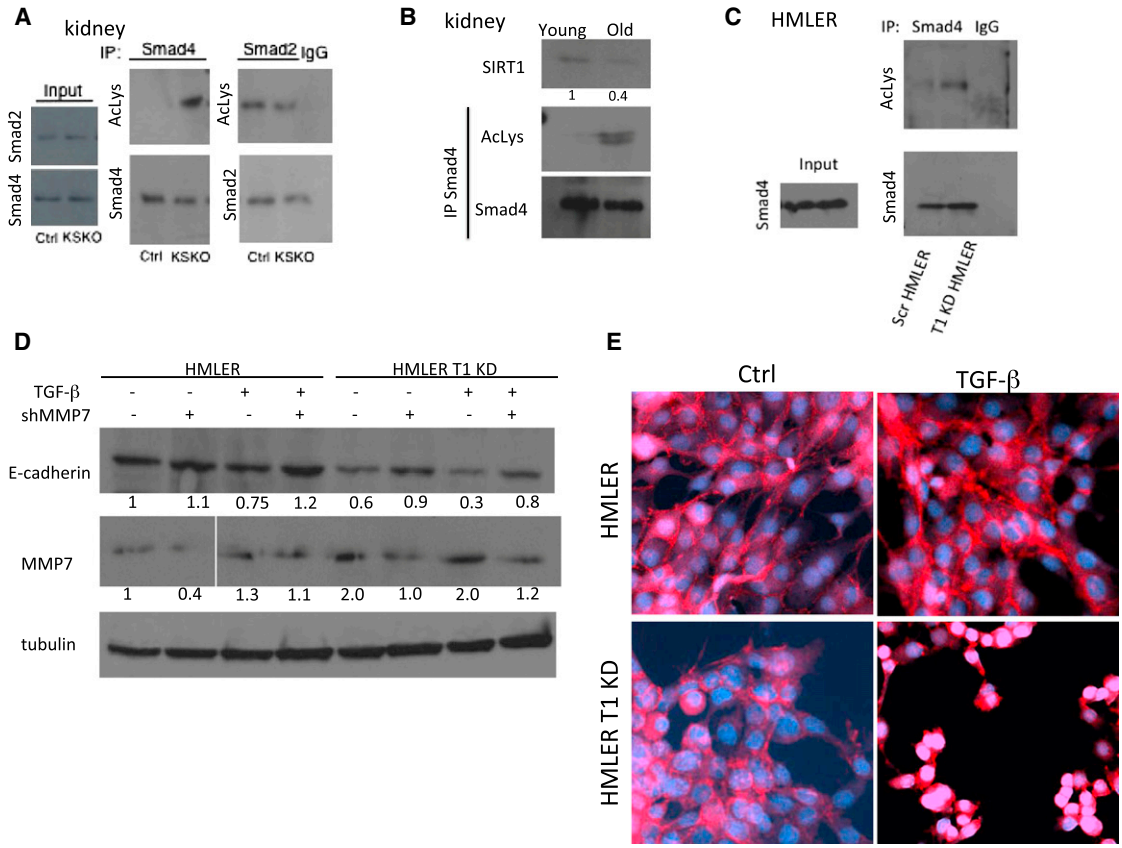

Figure 4. SIRT1 Deacteylates Smad4 Repressing the Activity of MMP7 on E-Cadherin Cleavage and β-Catenin Cellular Translocation

(A) Western blot of kidney samples 6 days following the AKI. Kidney samples were immunoprecipitated with Smad4 and Smad2 antibody or immunoglobulin G (IgG), and the blots were probed with acetyl-lysine (AcLys), Smad2, and Smad4 antibodies.

(B) Western blot of kidneys from 2 year (old) and 3 month (young) animals, probed with SIRT1 and immunoprecipitated with Smad4 or IgG and probed with acetyl-lysine antibody. Numbers below lanes are quantification by ImageJ, shown as a fold change in band intensity normalized to young kidneys.

(C) Western blot of HMLER cells immunoprecipitated with antibody or immunoglobulin G (IgG). Blots were probed with acetyl-lysine (AcLys) and Smad4 antibodies.

(D) Western blots of HMLER control and HMLER SIRT1 KD cells treated with TFG-β 5 ng/ml for 48 hr and transfected with shMMP7, as indicated. Blot was probed with E-cadherin, MMP-7, and tubulin antibodies. Numbers below lanes are quantification by ImageJ, shown as a fold change in band intensity normalized to HMLER cells without TGF-β treatment and shMMP7 transfection.

(E) Immunofluorescent staining for β-catenin of HMLER and HMLER SIRT1 KD cells treated with TGF-β (5 ng/ml), as indicated. The images show a slice through the nuclei of cells analyzed by confocal microscopy. Analysis of images stacks confirmed nuclear localization in the SIRT1 knockdown HMLER cells but not control HMLER cells.

See also Figure S4.

Finally, we do not believe that the effect of SIRT1 on metastasis occurs via p53. HMLER cells are transfected with SV40, and the expressed T antigen is known to inactivate p53. Indeed, doxycyline was not able to induce p21, a p53 target, in HMLER cells, while serving as a potent inducer in 143b control cells (Figure S5).

DISCUSSION

Our results show that reduction of SIRT1 promotes metastasis of breast epithelial cells in an orthotopic model of breast cancer and promotes EMT and cell motility in these cells in vitro. Further, EMT could be induced in both breast epithelial and kidney epithelial cells in vitro, and this was also repressed by SIRT1. These effects were associated with the hyperactivation of TGF-β and hyperacetylation of Smad4 in the absence of SIRT1, leading to an increase in expression of MMP7, which we demonstrate is a Smad4 target. We suggest that the absence of SIRT1 leads to MMP7 hyperexpression and degradation of E-cadherin from the cell surface, thereby releasing β-catenin from the cadherin junctions to the nucleus, which is the characteristic of mesenchymal cells (Figures 5A and 5B).

The literature suggests that the role of SIRT1 in cancer may depend on the tumor type. SIRT1 has been shown to protect against gut carcinomas in APCmin mice (Firestein et al., 2008), as well as tumorigenesis in $p53^{+/-}$ mice (Wang et al., 2008; Vaziri et al., 2001). However, SIRT1 was associated with malignancy in prostate cancer and chronic myelogenous leukemia (Byles et al.,

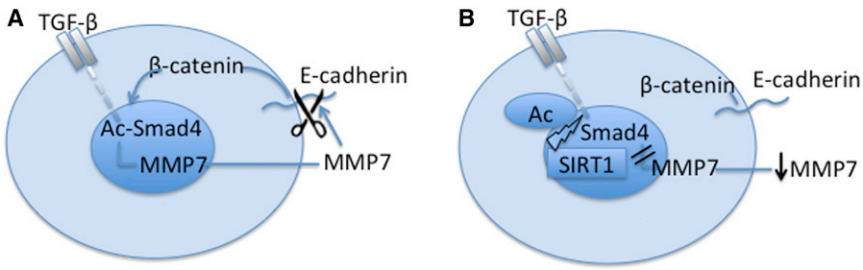

Figure 5. Schematic Representation of SIRT1 Effects on EMT
(A and B) Without SIRT1 (A) and with SIRT1 (B).

2012; Li et al., 2012). In prostate cancer, SIRT1 enhanced cell migration and metastasis after PC3 cancer cell tail injections by cooperating with EMT transcription factor ZEB1 to suppress E-cadherin transcription (Byles et al., 2012). The SIRT1 activator compound 1720 was shown to increase lung metastasis of implanted breast cancer cells, but EMT as a possible mechanism was not addressed (Suzuki et al., 2012). In normal mouse mammary epithelial cells, miR-200a negatively regulated SIRT1 expression and reduced EMT (Eades et al., 2011). However, an opposite role in cancer metastasis was indicated by the demonstration that miR-520c and miR-373 suppressed SIRT1 translation leading to increased expression of MMP9 and enhanced cell migration of fibrosarcoma cells (Liu and Wilson, 2012). To further confirm our data in animal studies, we performed the meta-analysis of human breast cancer trials and have shown that SIRT1 is downregulated in human invasive breast cancers.

Because of these seemingly conflicting data on SIRT1 in cancer, we employed a radically different model to follow up the cancer studies—fibrosis following kidney injury. Renal fibrosis after injury was mitigated in mice overexpressing SIRT1 in the kidney tubular epithelial cells and exacerbated in mice with *SIRT1* knocked out in those cells. This repression of fibrosis was due to repression of TGF-β signaling. For years it was believed that EMT is a major mechanism of renal fibrosis. However, a more recent study using fate tracing showed that epithelial cells do not give rise to interstitial myofibroblasts in wild-type mice following injury (Humphreys et al., 2010). We were able to confirm that EMT did not occur in fibrotic tissue of wild-type animals after injury. However, in the absence of SIRT1, 36% of interstitial myofibroblasts expressed the epithelial marker Hoxb7cre, suggesting their epithelial origin.

We also found long-term protective effects of SIRT1 after AKI in the progression to chronic disease. Previous studies had demonstrated SIRT1 protection using acute models of injury. For example, transgenic mice were protected against apoptosis of kidney tubular epithelium (Hasegawa et al., 2010), but $SIRT1^{+/-}$ heterozygotes were more susceptible to damage of medullar interstitial cells (He et al., 2010). In addition, calorie restriction protected against hypoxic AKI by increasing SIRT1 levels (Kume et al., 2010), and pharmacological activation of SIRT1 was also protective (Hasegawa et al., 2010; Lee et al., 2010; Li et al., 2010a; Funk et al., 2010).

SIRT1 represses the TGF-β signaling pathway important in EMT. TGF-β promotes differentiation and activation of myofibroblasts, which trigger scar and fibrous tissue formation and facilitate cancer progression and metastasis (Wendt et al., 2009). Further, TGF-β stimulation of EMT has been associated with the selection and expansion of breast cancer stem cells (Mani et al., 2008; Morel et al., 2008; Ben-Porath et al., 2008). Our results show that SIRT1 deacetylates and represses Smad4 in the TGF-β pathway, which lowers the expression of target genes. A previous study showed that SIRT1 deacetylated the negative regulator of TGF-β signaling, Smad7, to destabilize the protein in a mesangial kidney cell line (Kume et al., 2007). Were this to occur in the tubular epithelial cells in vivo, it might be expected to counteract the effect of SIRT1 on TGF-β signaling due to repression of Smad4. Our data indicate that the net effect of SIRT1 is to repress the output TGF-β pathway in tubular epithelial cells, suggesting that effects of this sirtuin on Smad7 are at best minor in these cells.

We also show that TGF-β regulates MMP7 expression, which is hyperexpressed when Smad4 is hyperacetylated in the absence of SIRT1. Further supporting the relationship between Smad4 and MMP7, MMP7 becomes dispensable for invasion in Smad4-deficient adenocarcinomas (Kitamura et al., 2009). MMP7 releases 80 kDa ectodomain fragment of E-cadherin (Noë et al., 2001), and we show a reduction of E-cadherin by MMP7 cells lacking SIRT1. Since disruption of E-cadherin by MMPs can mediate EMT (Zheng et al., 2009), metastasis (Onder et al., 2008), and cause nuclear translocation of β-catenin (Zheng et al., 2009; Onder et al., 2008), SIRT1 also leads to repression of a second pathway involved in EMT, Wnt signaling.

Interestingly, MMP7 levels increase in aging breast epithelial cells, which may contribute to age-associated breast cancer development (Chaturvedi and Hass, 2011). MMP7 levels also increase in tubular epithelial cells with age (Chen et al., 2007). As we show a decrease in SIRT1 levels and a corresponding increase in Smad4 acetylation in aged kidneys, it is interesting to speculate that the effect of MMP7 may be due to loss of SIRT1 activity in aging tissues.

In conclusion, SIRT1 reduces EMT in cancer and fibrosis by deacetylating Smad4 and repressing the effect of TGF-β signaling on MMP7. Consequently, less E-cadherin is cleaved from the cell surface and β-catenin remains bound to E-cadherin at the cell-cell junctions. These findings suggest that SIRT1 may be a target for prevention or possibly treatment of cancer metastasis and organ fibrosis.

EXPERIMENTAL PROCEDURES

Mouse Strains

Severe combined immunodeficiency mice were purchased from Charles River Laboratories. All other mice were in congenic C57Bl/6 background. KSKO mice were generated by crossing *SIRT1* allele containing a floxed exon 4 (Cheng et al., 2003) with Cre-expressing mice driven by the kidney epithelial collecting tubule-specific *Hoxb7cre* promoter (Jackson Laboratory). KSTG mice were generated by crossing *SIRT1 loxP*-flanked mice (Firestein et al., 2008) with mice having *Hoxb7cre* promoter. Ctrl Tg mice had no loxP locus

nor cre recombinase. All mice were housed at 25°C and 12:12 hr light/dark cycle. All experiments were performed in accordance to Massachusetts Institute of Technology guidelines and regulations and were approved by Committee on Animal Care.

Cells and Treatment

Immortalized tumorigenic primary human breast epithelial cells, HMLER cells (courtesy by R.A. Weinberg, Whitehead Institute), were maintained as described (Elenbaas et al., 2001). The *SIRT1*$^{+/+}$ and *SIRT1*$^{-/-}$ MEFs have been described (Lin et al., 2000). HK-2 cells were from ATCC. Cells were treated with 5 ng/ml TGF-β (Invitrogen) or aristocholic acid (Sigma) every other day for 2–8 days (Yang et al., 2010; Yu et al., 2002).

Plasmids and Cell Transfections

Stable cells were generated using lentivirus or retrovirus. The plasmids expressing mSIRT1 and PRRL-GFP vectors were purchased from Addgene, *Smad4*-shRNA, and pSM2 vector from Open Biosystems. siRNA-*SIRT1* plasmid has been previously described (Picard et al., 2004). Lentiviral vectors were made by pcr subcloning cDNA and ligating into pENTR-D-TOPO (Invitrogen). pENTR-D-TOPO vectors were sequenced and then the cDNA was transferred to pLenti4-TO-V5-DEST (Invitrogen) through recombination. Cells were then virally infected. Transient transfections were performed by using Fugene transfection reagent (Roche).

In Vivo Tumorigenesis and Metastasis Model

Severe combined immunodeficiency (SCID) mice (Charles River Laboratories) were used in these studies, and all the protocols were approved by the Massachusetts Institute of Technology Committee on Animal Care. Mice were anesthetized with isoflurane. Five million cells in PBS, diluted 1:2 with Matrigel (Beckton Dickinson), were injected into one mammary gland per female (Onder et al., 2008). Animals were sacrificed 7.5 or 8 weeks postinjection (depending when the primary tumors reached 2 cm in diameter), or sooner if they became moribund.

Meta-Analysis of Breast Cancer Clinical Trial

We performed meta-analysis of *SIRT1* expression in Oncomine database of breast cancers (http://www.oncomine.com). The analysis included 12 trials with 143 control and 1181 breast cancer tissues (Table S1). These 12 trials had 35 comparisons. We used the cutoff value of $p = 0.01$ for significance of SIRT1 expression change in any direction.

Acute Kidney Injury Model

Four-month-old mice (n = 12 per group) were subjected to ischemia-reperfusion model of AKI by clamping both renal pedicles for 30 min with vascular clips (Roboz) (Yang et al., 2010). Blood was collected throughout the experiment and kidneys at the end. Mice were sacrificed 6 days and 6 weeks following the AKI and experiment was repeated twice.

TGF-β Injections

TGF-β 100 μg/kg/day was injected intravenously to six mice/group for 4 days to induce kidney fibrosis. Mice were sacrificed on day 5 and kidneys were collected for analyses. The experiment was repeated twice.

Renal Function

Serum level of creatinine was measured by alkaline picrate, BUN by urease and potassium by ion-selective electrode method (Antech Diagnostics).

Histology, Histomorphometry, and Immunohistochemistry

Metastasis, kidney, bone, and adipose tissue histology was examined on formalin-fixed, paraffin-embedded sections 3 μm thick stained by hematoxylin-eosin and Masson's trichrome for kidneys (six sections/kidney). The degree of interstitial fibrosis was scored semiqantitatively on a 0–4 scale (0, no lesion; 1, <25%; 2, >25%–50%; 3, >50%–75%; 4, >75% of parenchyma affected by the lesion) (Yang et al., 2010). The collagen content of kidneys was quantified with the Sercol soluble collagen assay kit (Biocolor).

Vectastain kit (Vector Laboratories) and MM7 (Abcam) and large SV40 T antigen (Santa Cruz) antibodies were used to perform MMP7 staining of three consecutive kidney sections and large SV40 T antigen, used to transform HMLE cells, staining of tumor metastasis.

Immunofluorescent Staining

Kidney sections were labeled with antibody to α-SMA (Abcam) and collagen type IV. HMLER cells and HK-2 cells on coverslips were labeled with antibodies to E-cadherin (BD Transduction Laboratories), α-SMA, collagen type I and type IV (Abcam), vimentin (Abcam), and MMP7. HMLER cells were labeled with β-catenin antibody. The slides were exposed to Alexa Fluor 488, 568, and 594 anti-rabbit and anti-mouse secondary antibodies (Invitrogen). The staining was examined with fluorescence microscope (Zeiss AxioImager.M1). HMLER cells labeled with GFP were detected macroscopically after forming metastasis at necroscopy when organs were examined under a Leica MZ 12 fluorescence dissection microscope.

Western Blotting and Immunoprecipitation

Organs and cells were homogenized in RIPA buffer including Complete Protease Inhibitor (Roche). Protein (100 mg) was loaded onto SDS-PAGE gels and immunoblotted with anti-SIRT1 (Upstate), Smad2 (Abcam), Smad4 (Abcam), E-cadherin (Cell Signaling), MMP7 (Abcam), Acetyl-Lysine (Santa Cruz Biotechnology), and tubulin (Abcam) antibodies.

The immunoprecipitations were carried out by using Pierce Direct IP Kit (Thermo Scientific). To determine Smad2 and Smad4 acetylation, anti-Smad2, anti-Smad4, or normal rabbit serum were coupled to agarose beads, and then control, KSKO, KSTG kidney samples, HMLER control, and HMLER SIRT1 KD cells were incubated with the beads. The eluate was blotted with anti-Smad2, anti-Smad4, and anti-Acetyl-Lys antibodies.

Flow Cytometric Analysis and Sorting

Cell suspension from kidneys of control mice with cre-recombinase and KSKO mice after 4 days of treatment with TGF-β 100 μg/kg/day was prepared as described in Kitamoto et al. (2009). Following erythrocyte lysis, cells were resuspended in FACS buffer. Kidney cells were labeled using anti-α-SMA and anti-cre-recombinase primary antibodies and Alexa Fluor 488 and Alexa Fluor 647 secondary antibodies, counted by a FACSCalibur Flow Cytometer (BD Biosciences) and analyzed using FlowJo software (Ashland, OR). α-SMA-positive cells were sorted using FACSAria I (BD Biosciences).

RNA Isolation and Analysis

Total RNA from mouse kidneys and HMLER cells was isolated by using Trizol (QIAGEN). cDNA was synthesized from total RNA by SuperScript III reverse transcriptase (Invitrogen) with random primers. The cDNA was then subjected to real-time quantitative RT-PCR analysis with gene-specific primers in the presence of CYBR green (Bio-Rad). Relative abundance of mRNA was normalized to rpl19.

Chromatin Immunoprecipitation Analysis

Chromatin immunoprecipitation analysis from kidneys and HMLER cells was performed with Magna Chip kit (Millipore) by using Smad4 antibody (Abcam) and immunoglobulin (Ig) G. The primer sequences are in Table S2.

Luciferase Assay

Transcription of *Smad2-Smad4* was detected by transfecting MEFs with FM-SIM plasmid comprising of Smad-interacting motif (SIM) and Fast/FoxH1 motif (FM), which interacts with phospho-Smad2, fused to the Gal4 DNA-binding domain (Figure S5A) (Ross et al., 2006; courtesy of C. Hill, Cancer Research, UK). The *MMP7* promoter region responsive to Smad4 (−438 to −379) and a larger DNA promoter fragment (−660 to −216) were cloned into pGL3-basic vector luciferase plasmid (Addgene) by using Sac1 and XhoI restriction endonucleases (New England BioLabs). Cells were cotransfected with *MMP7* promoter-luciferase reporter and pRL-TK (Renilla luciferase; Promega) and treated with TGF-β 2 ng/ml for 48 hr. Luciferase activity was measured by Dual-Luciferase Reporter Assay System (Promega). The firefly luciferase activity was normalized to Renilla. The experiments were performed in triplicates and were repeated three times.

Statistical Analysis

The analyses were performed using ANOVA Dunnett test, except for survival, where log-rank test was used. Differences were considered significant if $p < 0.05$.

SUPPLEMENTAL INFORMATION

Supplemental Information includes five figures and two tables and can be found with this article online at http://dx.doi.org/10.1016/j.celrep.2013.03.019.

LICENSING INFORMATION

This is an open-access article distributed under the terms of the Creative Commons Attribution-NonCommercial-No Derivative Works License, which permits non-commercial use, distribution, and reproduction in any medium, provided the original author and source are credited.

ACKNOWLEDGMENTS

We are grateful to Caroline Hill for FM-SIM plasmid and Robert A. Weinberg for HMLER cell line. We wish to thank Benjamin Humphreys for advice and helpful discussions. This work is supported by Fulbright Association postdoctoral fellowship to P.S., American Cancer Society, Grant Number: PF-11-258-1-TBG to E.O.W., F32 CA 132358 to E.L.B., Ellison/AFAR postdoctoral research grant to M.B. and grants from the NIH and a gift from the Glenn Medical Foundation to L.G. L.G. is co-chair of the Senior Advisory Board for Sirtris/GSK.

Received: June 1, 2012
Revised: January 5, 2013
Accepted: March 14, 2013
Published: April 11, 2013

REFERENCES

Abrass, C.K., Adcox, M.J., and Raugi, G.J. (1995). Aging-associated changes in renal extracellular matrix. Am. J. Pathol. *146*, 742–752.

Ben-Porath, I., Thomson, M.W., Carey, V.J., Ge, R., Bell, G.W., Regev, A., and Weinberg, R.A. (2008). An embryonic stem cell-like gene expression signature in poorly differentiated aggressive human tumors. Nat. Genet. *40*, 499–507.

Brabletz, T., Jung, A., Spaderna, S., Hlubek, F., and Kirchner, T. (2005). Opinion: migrating cancer stem cells - an integrated concept of malignant tumour progression. Nat. Rev. Cancer *5*, 744–749.

Byles, V., Zhu, L., Lovaas, J.D., Chmilewski, L.K., Wang, J., Faller, D.V., and Dai, Y. (2012). SIRT1 induces EMT by cooperating with EMT transcription factors and enhances prostate cancer cell migration and metastasis. Oncogene *31*, 4619–4629.

Chaturvedi, S., and Hass, R. (2011). Extracellular signals in young and aging breast epithelial cells and possible connections to age-associated breast cancer development. Mech. Ageing Dev. *132*, 213–219.

Chen, G., Bridenbaugh, E.A., Akintola, A.D., Catania, J.M., Vaidya, V.S., Bonventre, J.V., Dearman, A.C., Sampson, H.W., Zawieja, D.C., Burghardt, R.C., and Parrish, A.R. (2007). Increased susceptibility of aging kidney to ischemic injury: identification of candidate genes changed during aging, but corrected by caloric restriction. Am. J. Physiol. Renal Physiol. *293*, F1272–F1281.

Cheng, H.L., Mostoslavsky, R., Saito, S., Manis, J.P., Gu, Y., Patel, P., Bronson, R., Appella, E., Alt, F.W., and Chua, K.F. (2003). Developmental defects and p53 hyperacetylation in Sir2 homolog (SIRT1)-deficient mice. Proc. Natl. Acad. Sci. USA *100*, 10794–10799.

Donmez, G., and Guarente, L. (2010). Aging and disease: connections to sirtuins. Aging Cell *9*, 285–290.

Eades, G., Yao, Y., Yang, M., Zhang, Y., Chumsri, S., and Zhou, Q. (2011). miR-200a regulates SIRT1 expression and epithelial to mesenchymal transition (EMT)-like transformation in mammary epithelial cells. J. Biol. Chem. *286*, 25992–26002.

Elenbaas, B., Spirio, L., Koerner, F., Fleming, M.D., Zimonjic, D.B., Donaher, J.L., Popescu, N.C., Hahn, W.C., and Weinberg, R.A. (2001). Human breast cancer cells generated by oncogenic transformation of primary mammary epithelial cells. Genes Dev. *15*, 50–65.

Ertel, A., Tsirigos, A., Whitaker-Menezes, D., Birbe, R.C., Pavlides, S., Martinez-Outschoorn, U.E., Pestell, R.G., Howell, A., Sotgia, F., and Lisanti, M.P. (2012). Is cancer a metabolic rebellion against host aging? In the quest for immortality, tumor cells try to save themselves by boosting mitochondrial metabolism. Cell Cycle *11*, 253–263.

Firestein, R., Blander, G., Michan, S., Oberdoerffer, P., Ogino, S., Campbell, J., Bhimavarapu, A., Luikenhuis, S., de Cabo, R., Fuchs, C., et al. (2008). The SIRT1 deacetylase suppresses intestinal tumorigenesis and colon cancer growth. PLoS ONE *3*, e2020.

Funk, J.A., Odejinmi, S., and Schnellmann, R.G. (2010). SRT1720 induces mitochondrial biogenesis and rescues mitochondrial function after oxidant injury in renal proximal tubule cells. J. Pharmacol. Exp. Ther. *333*, 593–601.

Guarente, L. (2011). Franklin H. Epstein Lecture: sirtuins, aging, and medicine. N. Engl. J. Med. *364*, 2235–2244.

Guarente, L., and Picard, F. (2005). Calorie restriction—the SIR2 connection. Cell *120*, 473–482.

Hasegawa, K., Wakino, S., Yoshioka, K., Tatematsu, S., Hara, Y., Minakuchi, H., Sueyasu, K., Washida, N., Tokuyama, H., Tzukerman, M., et al. (2010). Kidney-specific overexpression of Sirt1 protects against acute kidney injury by retaining peroxisome function. J. Biol. Chem. *285*, 13045–13056.

He, W., Wang, Y., Zhang, M.Z., You, L., Davis, L.S., Fan, H., Yang, H.C., Fogo, A.B., Zent, R., Harris, R.C., et al. (2010). Sirt1 activation protects the mouse renal medulla from oxidative injury. J. Clin. Invest. *120*, 1056–1068.

Humphreys, B.D., Lin, S.L., Kobayashi, A., Hudson, T.E., Nowlin, B.T., Bonventre, J.V., Valerius, M.T., McMahon, A.P., and Duffield, J.S. (2010). Fate tracing reveals the pericyte and not epithelial origin of myofibroblasts in kidney fibrosis. Am. J. Pathol. *176*, 85–97.

Imai, S., Armstrong, C.M., Kaeberlein, M., and Guarente, L. (2000). Transcriptional silencing and longevity protein Sir2 is an NAD-dependent histone deacetylase. Nature *403*, 795–800.

Ince, T.A., Richardson, A.L., Bell, G.W., Saitoh, M., Godar, S., Karnoub, A.E., Iglehart, J.D., and Weinberg, R.A. (2007). Transformation of different human breast epithelial cell types leads to distinct tumor phenotypes. Cancer Cell *12*, 160–170.

Kalluri, R., and Weinberg, R.A. (2009). The basics of epithelial-mesenchymal transition. J. Clin. Invest. *119*, 1420–1428.

Kim, K.K., Kugler, M.C., Wolters, P.J., Robillard, L., Galvez, M.G., Brumwell, A.N., Sheppard, D., and Chapman, H.A. (2006). Alveolar epithelial cell mesenchymal transition develops in vivo during pulmonary fibrosis and is regulated by the extracellular matrix. Proc. Natl. Acad. Sci. USA *103*, 13180–13185.

Kitamoto, K., Machida, Y., Uchida, J., Izumi, Y., Shiota, M., Nakao, T., Iwao, H., Yukimura, T., Nakatani, T., and Miura, K. (2009). Effects of liposome clodronate on renal leukocyte populations and renal fibrosis in murine obstructive nephropathy. J. Pharmacol. Sci. *111*, 285–292.

Kitamura, T., Biyajima, K., Aoki, M., Oshima, M., and Taketo, M.M. (2009). Matrix metalloproteinase 7 is required for tumor formation, but dispensable for invasion and fibrosis in SMAD4-deficient intestinal adenocarcinomas. Lab. Invest. *89*, 98–105.

Kume, S., Haneda, M., Kanasaki, K., Sugimoto, T., Araki, S., Isshiki, K., Isono, M., Uzu, T., Guarente, L., Kashiwagi, A., and Koya, D. (2007). SIRT1 inhibits transforming growth factor beta-induced apoptosis in glomerular mesangial cells via Smad7 deacetylation. J. Biol. Chem. *282*, 151–158.

Kume, S., Uzu, T., Horiike, K., Chin-Kanasaki, M., Isshiki, K., Araki, S., Sugimoto, T., Haneda, M., Kashiwagi, A., and Koya, D. (2010). Calorie restriction enhances cell adaptation to hypoxia through Sirt1-dependent mitochondrial autophagy in mouse aged kidney. J. Clin. Invest. *120*, 1043–1055.

Ledbetter, S., Kurtzberg, L., Doyle, S., and Pratt, B.M. (2000). Renal fibrosis in mice treated with human recombinant transforming growth factor-beta2. Kidney Int. *58*, 2367–2376.

Lee, M.J., Feliers, D., Sataranatarajan, K., Mariappan, M.M., Li, M., Barnes, J.L., Choudhury, G.G., and Kasinath, B.S. (2010). Resveratrol ameliorates high glucose-induced protein synthesis in glomerular epithelial cells. Cell. Signal. *22*, 65–70.

Li, J., Qu, X., Ricardo, S.D., Bertram, J.F., and Nikolic-Paterson, D.J. (2010a). Resveratrol inhibits renal fibrosis in the obstructed kidney: potential role in deacetylation of Smad3. Am. J. Pathol. *177*, 1065–1071.

Li, L., Zepeda-Orozco, D., Black, R., and Lin, F. (2010b). Autophagy is a component of epithelial cell fate in obstructive uropathy. Am. J. Pathol. *176*, 1767–1778.

Li, L., Wang, L., Li, L., Wang, Z., Ho, Y., McDonald, T., Holyoake, T.L., Chen, W., and Bhatia, R. (2012). Activation of p53 by SIRT1 inhibition enhances elimination of CML leukemia stem cells in combination with imatinib. Cancer Cell *21*, 266–281.

Lin, S.J., Defossez, P.A., and Guarente, L. (2000). Requirement of NAD and SIR2 for life-span extension by calorie restriction in Saccharomyces cerevisiae. Science *289*, 2126–2128.

Liu, P., and Wilson, M.J. (2012). miR-520c and miR-373 upregulate MMP9 expression by targeting mTOR and SIRT1, and activate the Ras/Raf/MEK/Erk signaling pathway and NF-κB factor in human fibrosarcoma cells. J. Cell. Physiol. *227*, 867–876.

Mani, S.A., Guo, W., Liao, M.J., Eaton, E.N., Ayyanan, A., Zhou, A.Y., Brooks, M., Reinhard, F., Zhang, C.C., Shipitsin, M., et al. (2008). The epithelial-mesenchymal transition generates cells with properties of stem cells. Cell *133*, 704–715.

Morel, A.P., Lièvre, M., Thomas, C., Hinkal, G., Ansieau, S., and Puisieux, A. (2008). Generation of breast cancer stem cells through epithelial-mesenchymal transition. PLoS ONE *3*, e2888.

Noë, V., Fingleton, B., Jacobs, K., Crawford, H.C., Vermeulen, S., Steelant, W., Bruyneel, E., Matrisian, L.M., and Mareel, M. (2001). Release of an invasion promoter E-cadherin fragment by matrilysin and stromelysin-1. J. Cell Sci. *114*, 111–118.

Nogueira, L.M., Dunlap, S.M., Ford, N.A., and Hursting, S.D. (2012). Calorie restriction and rapamycin inhibit MMTV-Wnt-1 mammary tumor growth in a mouse model of postmenopausal obesity. Endocr. Relat. Cancer *19*, 57–68.

Onder, T.T., Gupta, P.B., Mani, S.A., Yang, J., Lander, E.S., and Weinberg, R.A. (2008). Loss of E-cadherin promotes metastasis via multiple downstream transcriptional pathways. Cancer Res. *68*, 3645–3654.

Pannarale, G., Carbone, R., Del Mastro, G., Gallo, C., Gattullo, V., Natalicchio, L., Navarra, A., and Tedesco, A. (2010). The aging kidney: structural changes. J. Nephrol. *23*(*Suppl 15*), S37–S40.

Picard, F., Kurtev, M., Chung, N., Topark-Ngarm, A., Senawong, T., Machado De Oliveira, R., Leid, M., McBurney, M.W., and Guarente, L. (2004). Sirt1 promotes fat mobilization in white adipocytes by repressing PPAR-gamma. Nature *429*, 771–776.

Potenta, S., Zeisberg, E., and Kalluri, R. (2008). The role of endothelial-to-mesenchymal transition in cancer progression. Br. J. Cancer *99*, 1375–1379.

Ross, S., Cheung, E., Petrakis, T.G., Howell, M., Kraus, W.L., and Hill, C.S. (2006). Smads orchestrate specific histone modifications and chromatin remodeling to activate transcription. EMBO J. *25*, 4490–4502.

Singh, A., and Settleman, J. (2010). EMT, cancer stem cells and drug resistance: an emerging axis of evil in the war on cancer. Oncogene *29*, 4741–4751.

Suzuki, K., Hayashi, R., Ichikawa, T., Imanishi, S., Yamada, T., Inomata, M., Miwa, T., Matsui, S., Usui, I., Urakaze, M., et al. (2012). SRT1720, a SIRT1 activator, promotes tumor cell migration, and lung metastasis of breast cancer in mice. Oncol. Rep. *27*, 1726–1732.

Tapp, D.C., Kobayashi, S., Fernandes, G., and Venkatachalam, M.A. (1989). Protein restriction or calorie restriction? A critical assessment of the influence of selective calorie restriction on the progression of experimental renal disease. Semin. Nephrol. *9*, 343–353.

Tissenbaum, H.A., and Guarente, L. (2001). Increased dosage of a sir-2 gene extends lifespan in Caenorhabditis elegans. Nature *410*, 227–230.

Vaziri, H., Dessain, S.K., Ng Eaton, E., Imai, S.I., Frye, R.A., Pandita, T.K., Guarente, L., and Weinberg, R.A. (2001). hSIR2(SIRT1) functions as an NAD-dependent p53 deacetylase. Cell *107*, 149–159.

Viswanathan, M., and Guarente, L. (2011). Regulation of Caenorhabditis elegans lifespan by sir-2.1 transgenes. Nature *477*, E1–E2.

Wang, R.H., Sengupta, K., Li, C., Kim, H.S., Cao, L., Xiao, C., Kim, S., Xu, X., Zheng, Y., Chilton, B., et al. (2008). Impaired DNA damage response, genome instability, and tumorigenesis in SIRT1 mutant mice. Cancer Cell *14*, 312–323.

Wendt, M.K., Allington, T.M., and Schiemann, W.P. (2009). Mechanisms of the epithelial-mesenchymal transition by TGF-beta. Future Oncol. *5*, 1145–1168.

Yang, L., Besschetnova, T.Y., Brooks, C.R., Shah, J.V., and Bonventre, J.V. (2010). Epithelial cell cycle arrest in G2/M mediates kidney fibrosis after injury. Nat. Med. *16*, 535–543, 1p, 143.

Yao, D., Dai, C., and Peng, S. (2011). Mechanism of the mesenchymal-epithelial transition and its relationship with metastatic tumor formation. Mol. Cancer Res. *9*, 1608–1620.

Yu, J., Carroll, T.J., and McMahon, A.P. (2002). Sonic hedgehog regulates proliferation and differentiation of mesenchymal cells in the mouse metanephric kidney. Development *129*, 5301–5312.

Zeisberg, E.M., Tarnavski, O., Zeisberg, M., Dorfman, A.L., McMullen, J.R., Gustafsson, E., Chandraker, A., Yuan, X., Pu, W.T., Roberts, A.B., et al. (2007). Endothelial-to-mesenchymal transition contributes to cardiac fibrosis. Nat. Med. *13*, 952–961.

Zheng, G., Lyons, J.G., Tan, T.K., Wang, Y., Hsu, T.T., Min, D., Succar, L., Rangan, G.K., Hu, M., Henderson, B.R., et al. (2009). Disruption of E-cadherin by matrix metalloproteinase directly mediates epithelial-mesenchymal transition downstream of transforming growth factor-beta1 in renal tubular epithelial cells. Am. J. Pathol. *175*, 580–591.

Cell PRESS
Open ACCESS

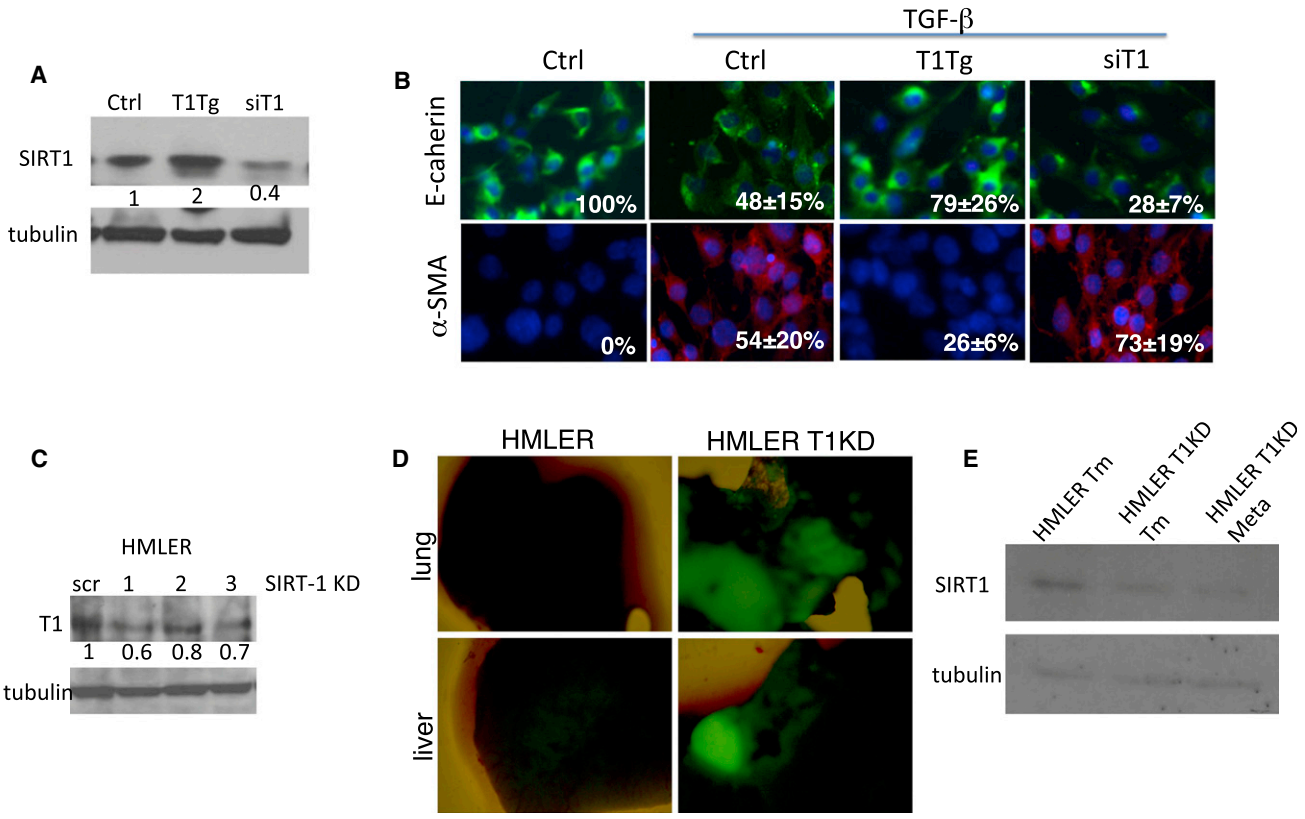

Figure S1. SIRT1 in Breast Cancer Cells, Related to Figure 1

(A) SIRT1 levels in HMLER cells. Western blot showing SIRT1 and tubulin protein in HMLER cells with SIRT1 knock-down (siT1) and overexpression (T1TG). Ctrl, control vector. Numbers below lanes are quantification by Image J, shown as a fold change in band intensity normalized to HMLER cells transfected with control vector.

(B) Immunofluorescence staining of MDA-MB231 cells with E-cadherin and α-SMA 4 days following the treatment with TGF-β 5 ng/ml (40x magnification, DAPI staining of nuclei). Numbers in the right bottom corners of images represent percentage of E-cadherin and α-SMA positive cells over total number of cells per slide (n = 3 slides per group), shown as average ± standard deviation, * significantly different from Ctrl treated with TGF-β, $p < 0.05$, ANOVA Dunnett test, T1Tg, MDA-MB231 cells overexpressing SIRT1; siT1, MDA-MB231 cells with knock-down for SIRT1, Ctrl, control MDA-MB231 cells.

(C) Western blot of HMLER cell lysates transfected with control vector (scr), or different constructs for SIRT1 KD (1-3), detected with SIRT1 and tubulin antibodies. Construct 1 was used for in vivo experiments. Numbers below lanes are quantification by Image J, shown as a fold change in band intensity normalized to scr.

(D) GFP images of metastases in HMLER cells and cells knocked down for SIRT1 (HMLER T1KD).

(E) SIRT1 levels in tumors and metastases. Western blots showing SIRT1 and tubulin in breast cancer and metastasis after implantation of HMLER and HMLER T1KD cells.

Cell PRESS
Open ACCESS

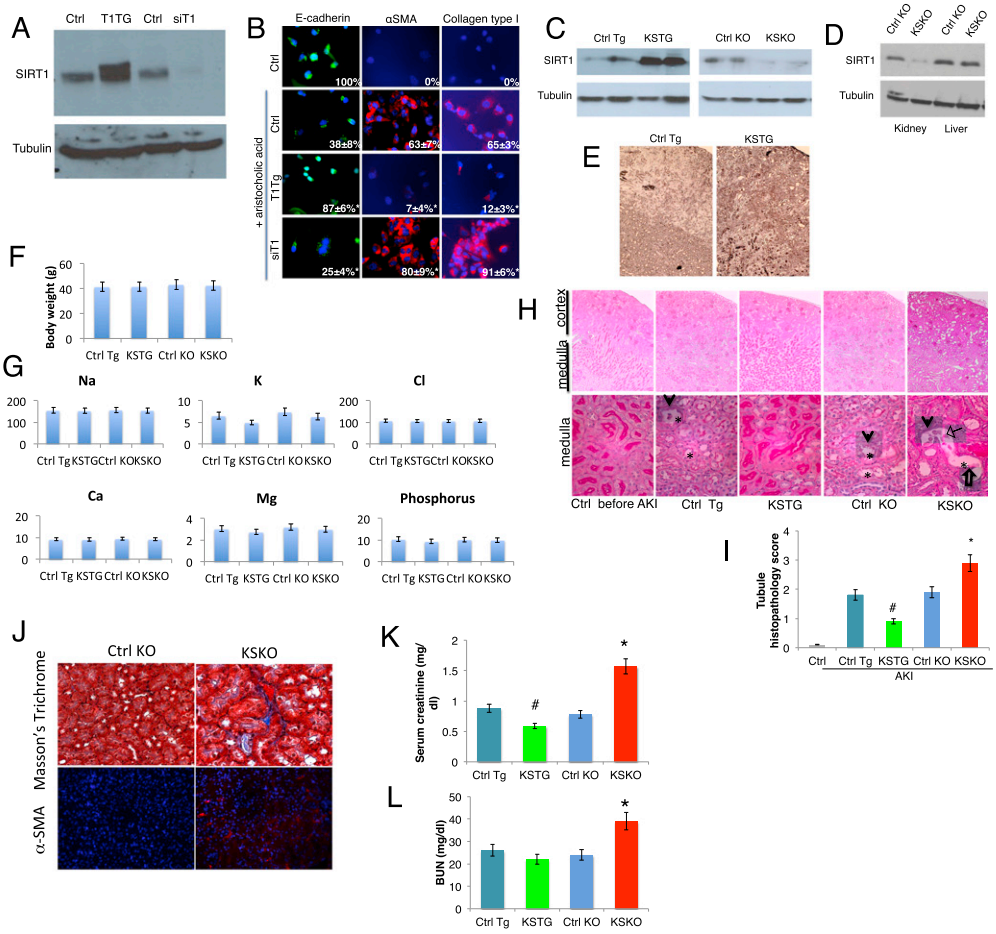

Figure S2. SIRT1 in Kidneys and Kidney Tubular Epithelial Cells, Related to Figure 2

(A) SIRT1 levels in HK-2 kidney epithelial cells. Western blot showing SIRT1 and tubulin protein in HK-2 kidney tubular epithelial cells with SIRT1 knock-down (siT1) and overexpression (T1TG). Ctrl, control vector.

(B) Immunofluorescent staining of HK-2 cells with E-cadherin, α-smooth muscle actin (α-SMA) and collagen type I 48 hr following the treatment with aristocholic acid 5μg/ml (63x magnification, DAPI staining of nuclei). Numbers in the right bottom corners of images represent percentage of E-cadherin, α-SMA or collagen type I positive cells over total number of cells per slide (n = 3 slides per group), shown as average ± standard deviation, * significantly different from Ctrl treated with aristocholic acid, $p < 0.05$, ANOVA Dunnett test, T1Tg, HK-2 cells overexpressing SIRT1; siT1, HK-2 cells with knock-down for SIRT1, Ctrl, control HK-2 cells.

(C) Western blot showing SIRT1 and tubulin protein in the medullary part of kidneys of specific kidney tubular SIRT1 knock-out (KSKO) and transgenic (KSTG) mice.

(D) Western blot showing SIRT1 and tubulin protein in the renal medulla and liver of specific kidney tubular SIRT1 knock-out (KSKO) and transgenic (KSTG) mice.

(E) Immunohistochemistry for SIRT1 in kidneys of Ctrl Tg and KSTG mice (magnification x10). Ctrl Tg, control for SIRT1 kidney specific transgenic mice; KSTG kidney specific transgenic mice; Ctrl KO, control for SIRT1 kidney specific knock-out mice.

(F and G) Basic phenotyping of KSKO and KSTG mice. (F) Body weights of KSKO and KSTG mice. (G) Electrolyte levels in blood of KSTG and KSKO mice. Na, sodium, K, potassium, Cl, chloride, Ca, calcium, Mg, magnesium and Phosphorus. Error bars represent s.d. Ctrl Tg, control for SIRT1 kidney specific transgenic mice; KSTG kidney specific transgenic mice; Ctrl KO, control for SIRT1 kidney specific knock-out mice, KSKO kidney specific knock-out mice.

(H) SIRT1 improves histological characteristics in AKI. Kidney histology at 6 days following the AKI (Periodic acid-Schiff staining). Upper row is low magnification (10x) showing cortex and outer medulla. Lower row is high magnification (63x) of tubules in outer medulla. Asterisk (*) shows dilated tubules, arrow points to flattened epithelial cells lacking nuclear staining, arrowhead shows debris in the tubular lumen and empty arrow shows fibroblasts protruding through the basement membrane to the tubular lumen.

(I) Tubule histopathology score (scoring system described in Experimental Procedures). * significantly different from Ctrl KO, # significantly different from Ctrl Tg, ANOVA Dunnett test (for all experiments except survival), $p \leq 0.05$. Error bars represent s.d. Ctrl Tg, control for SIRT1 kidney specific transgenic mice; KSTG kidney specific transgenic mice; Ctrl KO, control for SIRT1 kidney specific knock-out mice, KSKO kidney specific knock-out mice.

(J) Fibrosis in Ctrl KO and KSKO kidneys at baseline. Masson's trichrome and α-SMA immunofluorescent staining for myofibroblasts in red (magnification 20x, n = 6 per group).

(K) SIRT1 reduces progression to CKD.

(L) Serum creatinine values at 6 weeks following the AKI (n = 6 per group). (L) Blood urea nitrogen (BUN) values at 6 weeks following the AKI (n = 6 per group). * significantly different from Ctrl KO, # significantly different from Ctrl Tg, ANOVA Dunnett test, $p \leq 0.05$. Error bars represent s.d. Ctrl Tg, control for SIRT1 kidney specific transgenic mice; KSTG kidney specific transgenic mice; Ctrl KO, control for SIRT1 kidney specific knock-out mice, KSKO kidney specific knock-out mice.

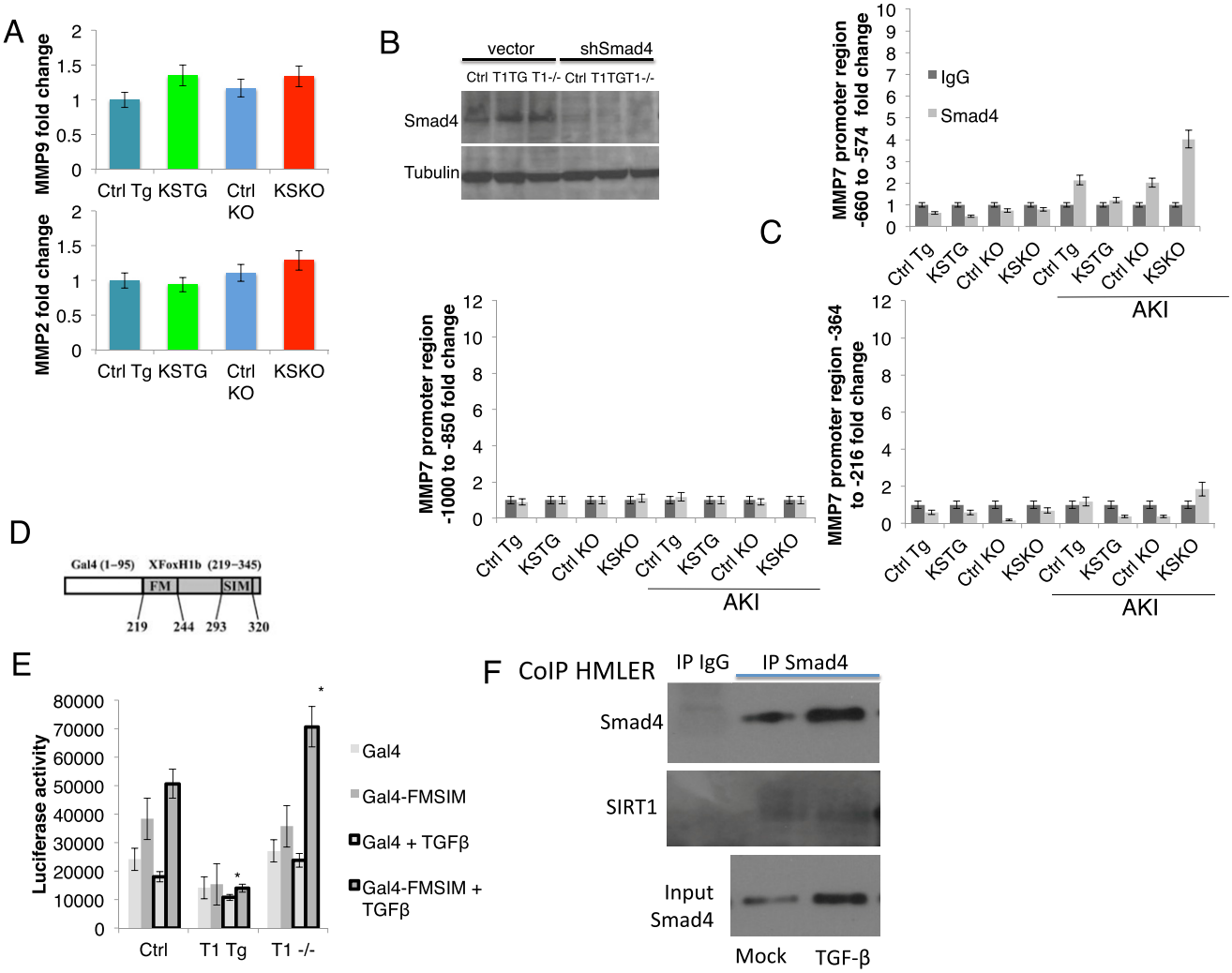

Figure S3. SIRT1 Affects MMP-7 via Smad4, Related to Figure 3

(A) SIRT1 does not affect MMP2 and MMP9 levels in kidneys following the AKI. qPCR gene expression of MMP2 and MMP9 in kidneys 6 days following the AKI. ANOVA Dunnett test, $p \leq 0.05$. Error bars represent s.d. Ctrl Tg, control for SIRT1 kidney specific transgenic mice; KSTG kidney specific transgenic mice; Ctrl KO, control for SIRT1 kidney specific knock-out mice, KSKO kidney specific knock-out mice.

(B) Smad4 levels in MEFs. Western blot showing Smad4 and tubulin protein in control (Ctrl), SIRT1 overxepressing (T1TG) and SIRT1 knock-down (T1−/−) MEFs transfected with Smad4 shRNA or empty vector (pSM2).

(C) The effect of SIRT1 on interaction of Smad4 with MMP7 promoter regions. Chromatin-immunoprecipitation on kidneys 6 days following the AKI with anti-Smad4 antibody or IgG. Different activity regions of the MMP7 promoter are tested by qPCR using the appropriate primers (see Table S2).

(D and E) SIRT1 reduces the transcription of Smad2-Smad4 complex in TGF-β pathway. (D) Schematic presentation of Gal4-FMSIM construct comprising of the C-terminal region of forkhead transcription factor, XFoxH1b, (interaction with Smad is mediated by Smad-interacting motif (SIM) and Fast/FoxH1 motif (FM), which interacts specifically with phosphorylated Smad2 complexes) fused to the Gal4 DNA-binding domain. (E) Luciferase assay of Gal4-FMSIM plasmid activity, showing the transcription of Smad2-Smad4 complex, as compared to Gal4 activity alone in mouse embryonic fibroblasts (MEFs) with stable overexpression of SIRT1 (T1Tg) and knock-down of SIRT1 (T1−/−). MEFs were treated with 2 ng/ml TGF-β for 48 hr. *, significantly different from control (Ctrl), $p < 0.05$.

(F) Co-immunoprecipitation of SIRT1 and Smad4. Western blot of HMLER cells. HMLER cells were immunoprecipitated with Smad4 or IgG antibody and the blots were probed with SIRT1 and Smad4 antibody.

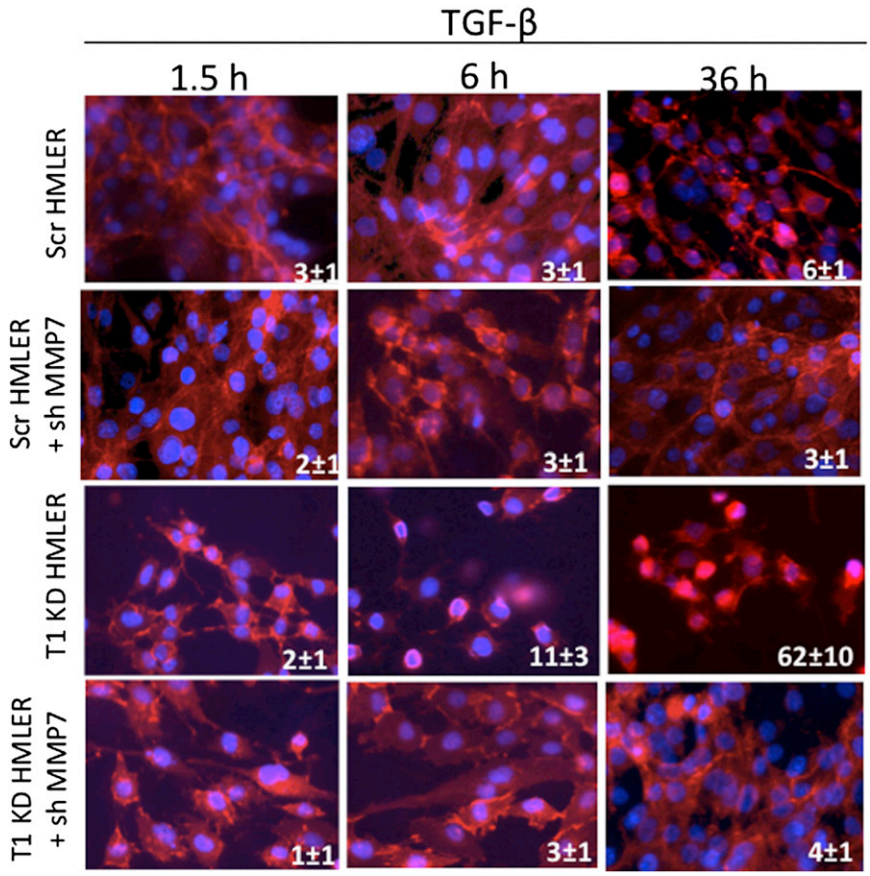

Figure S4. Immunofluorescent Staining for β-catenin of HMLER and HMLER SIRT1 KD Cells Treated with TGF-β (5 ng/ml) and MMP7 shRNA, as Indicated, Related to Figure 4

Numbers in panel corners are percentage of nuclear localization of β-catenin as compared to total cell number, presented as average ± SD.

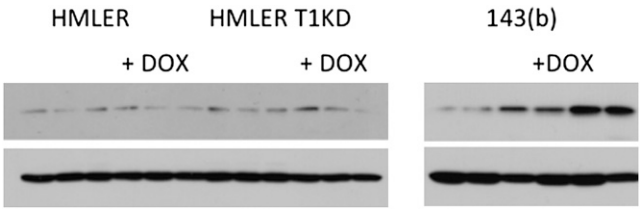

Figure S5. There Is No Induction of p53 in HMLER Cells, Related to Figure 4

Western blot of HMLER cells treated with doxycycline and probed with the p53 target p21 and β-actin.